

# Electrospray MS/MS reveals extensive and nonspecific oxidation of cholesterol esters in human peripheral vascular lesions<sup>[S]</sup>

Patrick M. Hutchins,\* Ernest E. Moore,<sup>†</sup> and Robert C. Murphy<sup>1,\*</sup>

Departments of Pharmacology\* and Surgery,<sup>†</sup> University of Colorado at Denver, Aurora, CO 80045

**Abstract** Although LDL is rendered proatherogenic by various experimental treatments (e.g., acetylation), the exact structural changes that drive LDL transformation in vivo remain enigmatic. Among the many hypothesized targets of oxidative modification are cholesterol esters (CE). This family of neutral lipids, which carries a highly unsaturated pool of fatty acyl groups, is the main component of both LDL particles and atherosclerotic plaques. Tandem mass spectrometry (MS/MS) was employed to reveal abundant and diverse oxidized CEs (oxCE), including novel oxidation products, within human peripheral vascular lesions. These oxCE species composed up to 40% of the total CE pool, with cholesteryl linoleate being oxidized to the greatest extent. Imaging mass spectrometry studies showed that oxCE was entirely confined within the plaque, along with unmodified CE and triacylglyceride (TAG). Interestingly, we found no evidence for TAG oxidation, although polyunsaturated species were abundant. Enzymatic oxidation of cholesteryl linoleate by 15-lipoxygenase (15-LO), an enzyme often invoked in CE oxidation, initially results in a regio- and stereospecific product.<sup>[1]</sup> Analysis of intact cholesteryl hydroxyoctadecadienoate isomers in human atheromata revealed no regio- or stereospecificity, indicating 15-LO was either not a major source of oxCE or nonenzymatic processes had eroded any product specificity.—Hutchins, P. M., E. E. Moore, and R. C. Murphy. **Electrospray MS/MS reveals extensive and nonspecific oxidation of cholesterol esters in human peripheral vascular lesions.** *J. Lipid Res.* 2011. 52: 2070–2083.

**Supplementary key words** atherosclerosis • 15-lipoxygenase • imaging mass spectrometry • MALDI • ammonium adduct • sodium adduct • triacylglyceride

The accumulation of neutral lipid in the arterial wall is a defining feature of atherosclerosis, and since the 1950s, oxidized lipid species within arterial plaques have been

reported (1, 2). Cholesteryl esters (CE) constitute the bulk of the accumulated neutral lipid, and a number of studies have identified several families of oxidized cholesteryl esters (oxCE). These oxCE species include hydroxy-octadecadienoate-CE (HODE-CE), hydroperoxy-octadecadienoate-CE (HpODE-CE), and oxo-octadecadienoate-CE (oxoODE-CE), as well as chain-shortened  $\omega$ -aldehyde-CE, often referred to as “core aldehydes” (3–6).

Oxidation of CE is frequently cited in the context of the oxidative modification theory of atherogenesis (7, 8). This well-supported theory proposes that LDL is oxidized and subsequently taken up by macrophages through surface receptors other than the LDL-receptor. This unregulated process leads to foam cell formation and atherogenesis. There is evidence that oxidation of CE, the chief component of LDL, may be involved in this process (9). First, abundant oxCE has been detected and shown to accumulate in human atheromata (4, 10). Oxidized CE has also been detected in human plasma (11). Second, CE is readily oxidized when LDL is incubated with macrophages (12). Finally, LDL particles oxidatively modified by macrophages are taken up at much greater rates than are unmodified LDL particles (13). For these reasons, a proatherogenic role of CE oxidation is widely assumed, although recent studies using foam cells as well as in vivo models suggested that oxidation of CE may increase reverse cholesterol transport; however, this hypothesis is controversial (3, 14, 15).

Abbreviations: BSTFA, *N,O*-bis(trimethylsilyl)-trifluoroacetamide; CE, cholesteryl ester; oxCE, oxidized cholesteryl ester; CID, collisionally induced decomposition; DCM, dichloromethane; EpOME, epoxy-octadecenoate; HETE, hydroxy-eicosatetraenoate; HODE, hydroxy-octadecadienoate; HpETE, hydroperoxy-eicosatetraenoate; HpODE, hydroperoxy-octadecadienoate; IMS, imaging mass spectrometry; 15-LO, 15-lipoxygenase; MRM, multiple reaction monitoring; MTBE, methyl tert-butyl ether; NH<sub>4</sub>OAc, ammonium acetate; NP, normal phase; oxoODE, oxo-octadecadienoate; RP, reversed phase; TAG, triacylglyceride; TOF, time of flight.

To whom correspondence should be addressed.

e-mail: Robert.Murphy@ucdenver.edu

<sup>[S]</sup> The online version of this article (available at <http://www.jlr.org>) contains supplementary data in the form of six figures and one table.

This work was supported in part by the LIPIDMAPS Large Scale Collaborative Grant GM-069338 from the General Medical Sciences Institute of the National Institutes of Health. Its contents are solely the responsibility of the authors and do not necessarily represent the official views of the National Institutes of Health or other granting agencies.

Manuscript received 29 July 2011 and in revised form 26 August 2011.

Published, JLR Papers in Press, August 31, 2011

DOI 10.1194/jlr.M019174

Production of oxCE and the consequences of its accumulation are likely complex, especially in the milieu of a multifactorial disease such as atherosclerosis. Certainly, the diverse and ever-expanding array of CE oxidation products has complicated efforts to investigate this phenomenon. To more completely characterize the nature of CE oxidation in atherosclerosis, we used HPLC-MS/MS to structurally elucidate oxCE species isolated from human atheromata. These analyses revealed a large array of abundant oxCE species, including novel oxidation products. It was immediately clear that this family of compounds was both more diverse and more abundant than previously appreciated. Interestingly, we found no evidence of triacylglyceride (TAG) oxidation in lesion extracts, even though polyunsaturated species were abundant and were shown to colocalize with oxCEs by imaging mass spectrometry (IMS). Note that several of the oxCE species identified in femoral and popliteal lesions have also been detected in iliac and carotid plaques and even in cholesterol-fed zebrafish (3–5, 16). These data suggest that the array oxCE species reported here might be common to advanced lesions throughout the vasculature.

15-Lipoxygenase (15-LO) was named for its ability to add an oxygen molecule to carbon fifteen of arachidonic acid. This is perhaps a misnomer as cholesteryl linoleate (18:2-CE) is the preferred substrate of 15-LO in vitro (17, 18). This enzymatic reaction results mainly in the formation of cholesteryl (*S*)-13-hydroxy-9Z,11E-octadecadienoate ((*S*)-13-(ZE)-HODE-CE). 15-LO is expressed in lesions (19), and several studies have investigated its potential activity by analyzing CEs for this chiral oxidation product. These efforts have produced conflicting results (5, 20–22). Here, chiral analysis of intact oxCE species in human lesions found no preponderance of the 15-LO-specific product.

## EXPERIMENTAL PROCEDURES

### Materials

Cholesteryl (+/–)-13-hydroxy-9Z,11E-octadecadienoic acid (13-(ZE)-HODE-CE), (*R*)-13-(ZE)-HODE-CE, and (+/–)-9-hydroxy-10E,12Z-octadecadienoic acid (9-(EZ)-HODE-CE) were obtained from Cayman Chemical (Ann Arbor, MI). Also purchased from Cayman Chemical were cholesteryl (+/–)-13-hydroperoxy-9Z,11E-octadecadienoic acid (13-(ZE)-HpODE-CE) and (+/–)-9-hydroperoxy-10E,12Z-octadecadienoic acid (9-(EZ)-HpODE-CE) as a mixture. Cholesteryl 9Z-heptadecenoate was obtained through Avanti Polar Lipids (Alabaster, AL). Custom-synthesized d4-17,17,18,18-linoleic acid was supplied by Dr. Howard Sprecher (23). The *N,O*-bis(trimethylsilyl)-trifluoroacetamide (BSTFA) was purchased from Supelco (Bellefonte, PA). Methoxyamine hydrochloride was obtained from MP Biomedicals (Solon, OH). Polymer-supported carbodiimide beads were purchased from Biotage (Uppsala, Sweden). The free fatty acids 13-oxo-9Z,11E-octadecadienoate (13-OxoODE), 9-oxo-10E,12Z-octadecadienoate (9-OxoODE), and 11-hydroxy-5Z,8Z,12E,14Z-eicosatetraenoate (11-HETE) were purchased from Cayman Chemical, as was purified soybean 15-lipoxygenase. Free cholesterol was obtained from Sigma-Aldrich (St. Louis, MO). All solvents used were HPLC or Optima grade and were obtained from

Sigma-Aldrich or Fischer Scientific (Fair Lawn, NJ). Protocol Hema 3<sup>®</sup> histology stain set was purchased from Fisher Scientific.

### Human samples

Data are presented from six atheromata samples originating from four subjects. Three samples were generated during femoral endarterectomy procedures on two individual patients. Three unique lesions were recovered from the popliteal arteries of two patients. Samples were immediately frozen (–80°C) after collection, and the elapsed time until extraction was kept to a minimum, usually <24 h. These samples constitute discarded tissue generated during medical procedures and were collected from patients with informed consent. Additional approval from the Colorado multi-institutional review board was granted for the transfer of deidentified tissue samples to this laboratory for analysis. Pooled human plasma (from 22 volunteer donors) was assembled at the University of Texas Southwestern Medical Center (Dallas, TX) and transferred to the laboratory at the University of Colorado Denver with institutional approval.

### Atheromata preparation

Samples were stored at –70°C before analysis. Once thawed, atheromata were placed in a 1 ml etched glass tissue grinder containing 1 ml of 1:1 MeOH:H<sub>2</sub>O (v/v) and homogenized over ice. Certain samples were spiked with internal standard(s) prior to homogenization. Homogenate was extracted twice using 500 µl 75:25 isooctane:ethyl acetate (v/v). The combined organic layers were dried under N<sub>2</sub>, and then the residue was weighed, diluted to 1 µg/µl in isooctane, and stored at –20°C. Auto-oxidation during homogenization/extraction was assessed. In certain experiments, atheromata tissue was homogenized and extracted in the presence of d<sub>4</sub>-18:2-CE at approximately equal concentration as endogenous 18:2-CE. Oxidation products of endogenous 18:2-CE were clearly detected; however, no oxidation of the d<sub>4</sub>-18:2-CE was observed (supplementary Fig. II). To monitor oxidation postextraction, identical analyses were performed on a single sample immediately following extraction and again after 75 days of storage at –20°C. The ratio of HODE-CE / 18:2-CE (by raw peak area) was unchanged over time: 1.57 at day 0 and 1.54 at day 75, indicating undetectable oxidation during this storage period.

### Chromatography

Normal-phase HPLC (NP-HPLC) was performed essentially as previously reported (24). For most analyses, 1–10 µg of lipid residue was injected. For preparative chromatography, up to 100 µg of lipid was loaded onto a 250 × 4.6 mm, 5 µm, Ultramex Silica column from Phenomenex. The same gradient and solvents were used but at a flow of 1 ml/min, of which approximately 200 µl was introduced into the mass spectrometer while the remainder was diverted to a fraction collector.

### Chiral separations

HPLC was performed on a 250 × 4.6 mm Chiracel<sup>®</sup> OD, cellulose-tris (3,5-dimethylphenylcarbamate), 10 µm silica-gel column from Chiral Technologies Inc. (West Chester, PA). 13-(ZE)-HODE-CE was isolated from 25 µg of total lipid. (*R*)- and (*S*)-13-(ZE)-HODE-CE were separated using a gradient of methyl tert-butyl ether (MTBE) in isooctane (700 µl/min), starting at 35% MTBE and ramping to 47% over 20 min.

Reversed-phase HPLC (RP-HPLC) was employed to separate hydrolyzed acyl components as previously reported (25). Acyl components derived from approximately 10–100 µg of total lipid were analyzed. Cholesteryl esters were saponified according to

the method of Parks et al. using NaOH (5% w/w) in 10:1 ethanol:H<sub>2</sub>O (26). The solutions were then acidified and free fatty acids were extracted with 2 × 500 μl 75:25 isooctane:ethyl acetate. If acidification was undesirable, free fatty acids were isolated by C<sub>18</sub> solid phase extraction as previously described (25).

### Oxidized cholesteryl ester derivatization and synthesis

Silylation of hydroxy- and hydroperoxy-CEs was done with BSTFA as follows. Two microliters of BSTFA was added to ~10 ng substrate in 50 μl ACN. The mixture was gently agitated for 1 min before the solution was evaporated under a stream of N<sub>2</sub> and diluted in 40 μl of isooctane. Ketones and aldehydes were converted to methoxime species using gaseous methoxyamine in a solvent-free reaction system as described previously (27). The derivatized products were extracted and diluted as described above.

For small-scale cholesteryl ester syntheses (>100 μg), various free fatty acids were esterified to cholesterol using PS-carbodiimide essentially as follows. One milligram of PS-carbodiimide beads was added to 1 μg of free fatty acid in 1 ml dichloromethane (DCM). After approximately 1 min of intermittent vortexing, 10 μg of free cholesterol in 200 μl DCM were added, and the vial was tumbled overnight at room temperature. The solution was then decanted into a sample vial, dried under a stream of N<sub>2</sub>, and diluted in 100 μl isooctane. For larger-scale cholesteryl ester syntheses, solution-phase coupling chemistry was employed as previously described (24).

### Mass spectrometry

Online NP-HPLC-MS/MS was performed on an AB Sciex API 3200 triple quadrupole mass spectrometer (AB Sciex, Toronto, Canada). Eluent from all normal-phase chromatographic methods was modified with 10 mM ammonium acetate (NH<sub>4</sub>OAc) in 95:5 acetonitrile:H<sub>2</sub>O (v/v) introduced prior to the ion source at a flow rate equal to one fifth that of the eluent. The mass spectrometer was operated in positive ion mode with an ion spray voltage of 5.5 kV. For most experiments, the mass spectrometer alternated between precursor ion scanning (precursors of *m/z* 369.3 or 385.3) and full mass Q3 scanning. Precursor ion data from *m/z* 620 to 780 (or *m/z* 420 to 620), was collected over 5 s periods with a collision energy of 18 V. Q3 scans from *m/z* 600 to 1000 were collected using no collision energy. Alternatively, CEs and oxCEs were detected by multiple reaction monitoring (MRM) in which 19 transitions were monitored for 200 msec each using the same parameters as precursor ion experiments (supplementary Table I). Collisionally induced decomposition (CID) spectra, from *m/z* 100 to 700, were collected online using parameters identical to precursor ion and MRM experiments.

CID spectra of hydrolyzed acyl components were also collected online during RP-HPLC. These experiments were performed on a Thermo Finnigan LTQ linear ion trap tandem mass spectrometer (San Jose, CA) operating in negative ion mode using data-dependent MS/MS. Eluent was introduced into the electrospray ion source at 200 μl/min, where the voltage was set at 4.5 kV and the capillary temperature was 150°C. The mass spectrometer alternated between full mass scanning (*m/z* 150 to 350) and MS/MS, using an isolation window of 1.8 amu and collision energy of 17 V with wideband activation.

### Quantitation of cholesteryl ester oxidation

Calibration curves were made for each of the three major CE species and to commercially available oxCE species (9- and 13-HODE-CE as well as 9- and 13-HpODE-CE) using 7.8 pmol of cholesteryl 9Z-heptadecenoate (17:1-CE) as a common internal standard (supplementary Fig. I). Aliquots of atheroma extract

were spiked with internal standard and analyzed by NP-HPLC-MS/MS using MRM. The analysis included MRM transitions for the internal standard, the three major CE species, and four families of oxidation products for each major CE. These included CE + oxygen (M + 16 amu), CE + oxygen – H<sub>2</sub> (M + 14 amu), CE + O<sub>2</sub> (M + 32 amu), CE + O<sub>2</sub> – H<sub>2</sub> (M + 30 amu) (supplementary Table I). As reference standards were not available to generate calibration curves for most oxCEs, an averaged calibration curve was used to normalize all oxCEs.

### MALDI IMS

Artery segments (3–5 mm) from human subjects were cut from still-frozen arteries to preserve gross morphology. Thawed samples were flushed with saline and embedded in modified OCT (28). Cross-sectional slices (20 μm) were placed on cover slips and lyophilized for 1 h. Slides were attached to the MALDI plate and dihydroxybenzoic acid was sublimed onto the entire surface as previously described (29). Images were acquired on a QSTAR XL quadrupole-time of flight (Q-TOF) mass spectrometer equipped with a MALDI ion source (Applied Biosystems/MDX Sciex, Thornhill, Ontario, Canada). Instrument parameters and data processing were described previously (28). For MALDI CID spectra of authentic CEs and oxCEs, standards were dried onto the MALDI plate from a 1 ng/μl solution in isooctane. A solution of NaCl (6 mM) in 1:1 MeOH:H<sub>2</sub>O (v/v) was then dried over the resulting spot before the entire plate was coated with DHB by sublimation.

IMS samples were stained with Hema 3<sup>®</sup> according to the manufacturer's guidelines following MALDI analysis. Adjacent sections were collected and fixed with 3% formaldehyde for 15 min, then rinsed with 60% isopropanol in H<sub>2</sub>O before staining for 15 min with a filtered solution of Oil Red O (5% w/w in 60% isopropanol:H<sub>2</sub>O) followed by rinsing and staining with the blue solution of the Hema 3<sup>®</sup> stain set.

### Statistics and data analysis

Chromatographic peaks were integrated and area ratios were generated using MultiQuant (ABSciex). Statistical analyses were performed using GraphPad Prism 4 (GraphPad Software, Inc.).

## RESULTS

### NP-HPLC-MS/MS separation of cholesteryl esters of human atheromata

Collisionally induced dissociation of ammoniated cholesteryl esters, [M+NH<sub>4</sub>]<sup>+</sup>, yields a strong cholesteryl cation at *m/z* 369, regardless of the acyl component (24). Therefore scanning for precursor ions of the *m/z* 369 fragment was a quasi-selective tandem mass spectrometry approach for the detection of CE species. In these analyses, complex mixtures of neutral lipids were extracted from homogenates of human atheromata, separated by NP-HPLC, and detected using this precursor ion method. As expected, unoxidized cholesteryl esters showed little retention on the silica column, with all species essentially coeluting just after the solvent front (Fig. 1). CEs were exclusively observed as ammoniated ions, the most abundant being 18:2-CE, followed by cholesteryl arachidonate (20:4-CE), and cholesteryl docosahexaenoate (22:6-CE). From 7 to 35 min, a series of increasingly polar oxCEs eluted. The *m/z* values of these oxCEs were consistent with the addition of one or two oxygen atoms to the most abundant CE species,



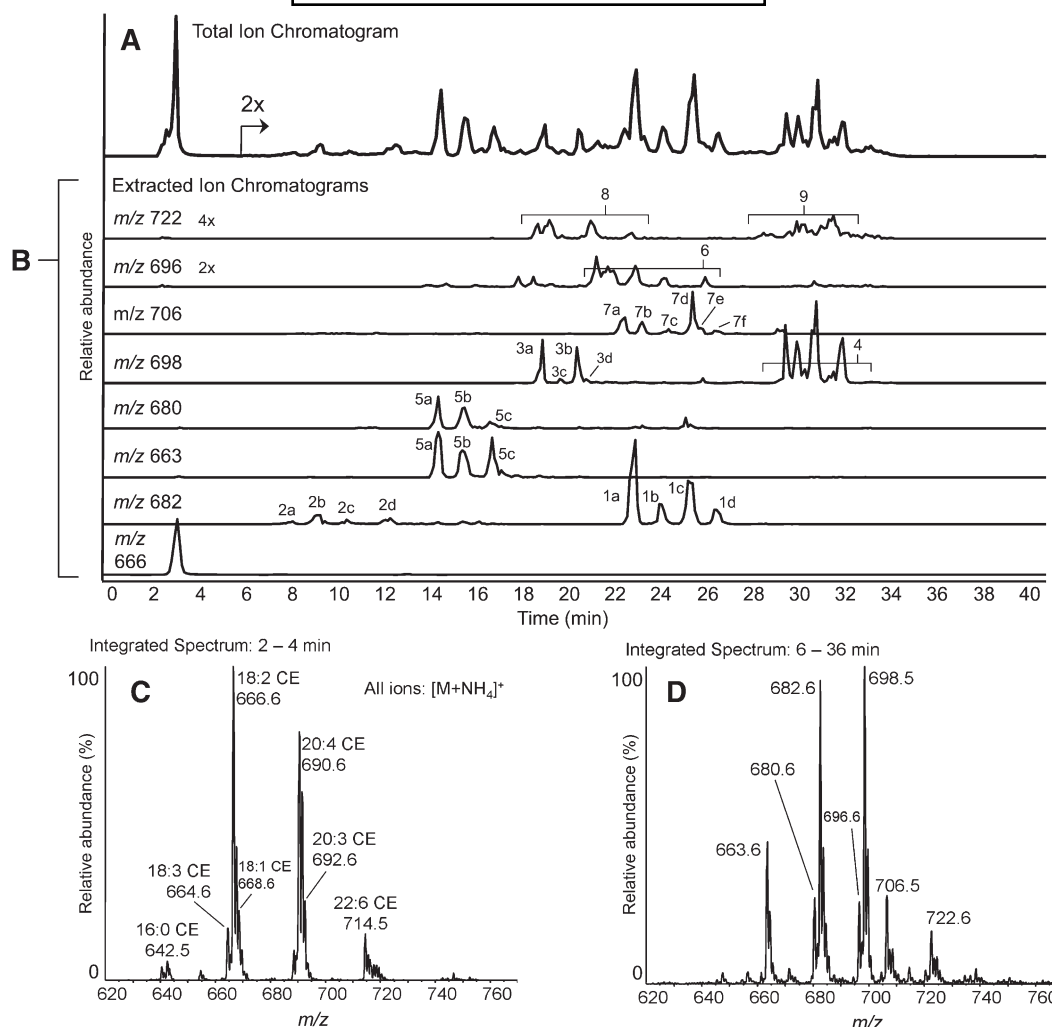


**Fig. 1.** NP-HPLC-MS/MS analysis of cholesteryl esters extracted from a human femoral endarterectomy atheroma sample. (A) Precursors of  $m/z$  369.3 ( $m/z$  620 to 780) total ion chromatogram. (B) Precursors of  $m/z$  369.3 extracted ion chromatograms of cholesteryl linoleate and major oxidized cholesteryl esters. Individual extracted ion chromatograms are labeled with the  $m/z$  value extracted. All chromatograms are normalized to the absolute signal for unoxidized cholesterol esters in panel A (set to 100% relative abundance), except as noted. (C) Integrated mass spectral data, averaged over the elution time of unoxidized cholesteryl ester species (2 to 4 min). CE species are labeled with  $m/z$  values and their acyl components by total acyl carbons and double bonds. (D) Integrated mass spectral data, averaged over the elution time of oxidized cholesteryl ester species (6 to 36 min). Oxidized CE species are labeled with  $m/z$  values.

18:2-CE and 20:4-CE (Fig. 1C, D). From the number of chromatographic peaks, it was obvious that a complex array of structurally diverse oxCEs was present. Isobaric, yet chromatographically separable, species indicated that there were likely several families of related isomers having the same empirical formulae. Oxidized CEs were generally observed as ammoniated ions; however, certain oxCEs appeared to form both ammoniated and protonated ion species (Fig. 1B,  $m/z$  680, 663).

The sections that follow describe the groups of peaks in the extracted ion chromatograms (Fig. 1B).

#### Group 1 peaks

The most abundant ion,  $m/z$  682, was consistent with the addition of a single oxygen atom (+16 amu) to 18:2-CE (Fig. 1B). The extracted ion chromatogram revealed a set

of four abundant peaks. Peaks 1a and 1c coeluted with commercially available authentic standards of 13-(ZE)-HODE-CE and 9-(EZ)-HODE-CE, respectively (data not shown). Peaks 1b and 1d were likely the all-*trans* isomers 13-(EE)-HODE-CE and 9-(EE)-HODE-CE, respectively, as previously determined (30). All group 1 peaks produced identical product ion spectra that exactly matched both HODE-CE standards. Isolated group 1 peaks were readily trimethylsilylated with BSTFA, resulting in an increase in mass (+72 amu) and a marked reduction in polarity (supplementary Fig. III-A). Individually isolated group 1 peaks were saponified, and the free acyl components were subjected to RP-HPLC MS/MS. The retention times and CID spectra of the carboxylate anions were consistent with the authentic HODEs. Group 1 peaks were HODE-CE isomers as indicated in **Table 1**.

TABLE 1. Major oxidized cholesteryl esters of human atheromata

Peak <sup>a</sup>	<i>m/z</i> <sup>b</sup>	Esterified Acyl Component <sup>c</sup>	Abbreviated oxCE Name <sup>d</sup>	Example Structure <sup>e</sup>
1a	682	13-hydroxy-9Z,11E-octadecadienoate <sup>c</sup>	13-(ZE)-HODE-CE	
1b	682	13-hydroxy-9E,11E-octadecadienoate	13-(EE)-HODE-CE	
1c	682	9-hydroxy-10E,12Z-octadecadienoate	9-(EZ)-HODE-CE	
1d	682	9-hydroxy-10E,12E-octadecadienoate	9-(EE)-HODE-CE	
2a	682	12,13-epoxy-9Z-octadecadienoate <sup>c</sup>	12,13-(E)-EpOME-CE	
2b	682	12,13-epoxy-9E-octadecadienoate	12,13-(Z)-EpOME-CE	
2c	682	9,10-epoxy-12Z-octadecadienoate	9,10-(E)-EpOME-CE	
2d	682	9,10-epoxy-12E-octadecadienoate	9,10-(Z)-EpOME-CE	
3a	698	13-hydroperoxy-9Z,11E-octadecadienoate <sup>c</sup>	13-(ZE)-HpODE-CE	
3b	698	13-hydroperoxy-9E,11E-octadecadienoate	13-(EE)-HpODE-CE	
3c	698	9-hydroperoxy-10E,12Z-octadecadienoate	9-(EZ)-HpODE-CE	
3d	698	9-hydroperoxy-10E,12E-octadecadienoate	9-(EE)-HpODE-CE	
4 <sup>†</sup>	698	13-hydroxy-9,10-epoxy-octadecadienoate <sup>c</sup>	13-hydroxy-9,10-EpOME-CE	
4 <sup>†</sup>	698	11-hydroxy-9,10-epoxy-octadecadienoate	11-hydroxy-9,10-EpOME-CE	
4 <sup>†</sup>	698	9-hydroxy-12,13-epoxy-octadecadienoate	9-hydroxy-12,13-EpOME-CE	
4 <sup>†</sup>	698	11-hydroxy-12,13-epoxy-octadecadienoate	11-hydroxy-12,13-EpOME-CE	
5a	680	13-oxo-9Z,11E-octadecadienoate <sup>c</sup>	13-(ZE)-oxoODE-CE	
5b	680	13-oxo-9E,11E-octadecadienoate	13-(EE)-oxoODE-CE	
5b	680	9-oxo-12E,13Z-octadecadienoate	9-(EZ)-oxoODE-CE	
5c	680	9-oxo-12E,13E-octadecadienoate	9-(EE)-oxoODE-CE	
6 <sup>†</sup>	696	13-oxo-9,10-epoxy-octadecadienoate <sup>c</sup>	13-oxo-9,10-EpOME-CE	
6 <sup>†</sup>	696	11-oxo-9,10-epoxy-octadecadienoate	11-oxo-9,10-EpOME-CE	
6 <sup>†</sup>	696	9-oxo-12,13-epoxy-octadecadienoate	9-oxo-12,13-EpOME-CE	
6 <sup>†</sup>	696	11-oxo-12,13-epoxy-octadecadienoate	11-oxo-12,13-EpOME-CE	
7a <sup>†</sup>	706	15-hydroxy-eicosatetraenoate <sup>c</sup>	15-HETE-CE	
7b <sup>†</sup>	706	12-hydroxy-eicosatetraenoate	12-HETE-CE	
7c <sup>†</sup>	706	11-hydroxy-eicosatetraenoate	11-HETE-CE	
7d <sup>†</sup>	706	9-hydroxy-eicosatetraenoate	9-HETE-CE	
7e <sup>†</sup>	706	8-hydroxy-eicosatetraenoate	8-HETE-CE	
7f <sup>†</sup>	706	5-hydroxy-eicosatetraenoate	5-HETE-CE	

<sup>a</sup> Refers to the labeled peaks of the extracted ion chromatograms shown in Figure 1B

<sup>b</sup> Nominal mass to charge ratio of ammoniated oxCE species, [M+NH<sub>4</sub>]<sup>+</sup>

<sup>c</sup> Indicated species are shown as example structures

<sup>d</sup> The immediate region surrounding the site acyl of component oxidation is shown; carbons are numbered from carboxyl carbon 1

<sup>e</sup> Double bond geometries not indicated in the species name are hypothetical

<sup>†</sup> Double bond geometry and stereochemistry were not determined

## Group 2 peaks

The early eluting peaks of *m/z* 682 were far less polar than the isobaric HODE-CE family (group 1) (Fig. 1B). The molecular weight and polarity of this oxCE family were consistent with a series of epoxy-octadecenoate-CEs (EpOME-CE). Group 2 peaks were collected individually, and the saponified acyl components were analyzed by RP-HPLC-MS/MS. The retention times and CID spectra of hydrolyzed peaks 2b and 2d matched authentic 12,13-(E)-EpOME and 9,10-(E)-EpOME, respectively. Hydrolyzed peaks 2a and 2c produced the same spectra as 2b and 2c, respectively, and were therefore hypothesized to be the *trans* isomers. Group 2 peaks were likely a series of EpOME-CEs as indicated in Table 1.

## Group 3 peaks

The second most abundant ion, observed at *m/z* 698, was consistent with addition a two oxygen atoms to 18:2-CE (+32 amu) (Fig. 1B). The extracted ion chromatogram of

*m/z* 698 revealed two sets of peaks. Group 3 consisted of four peaks eluting from 19 to 22 min. Peaks 3a and 3b coeluted with a authentic standard cholesteryl 13-(ZE)-HpODE-CE and 9-(EZ)-HpODE-CE, respectively. On the basis of previous separations of HpODE-CE mixtures, peaks 3c and 3d were likely the corresponding all *trans* isomers (30). Peaks 3a and 3b yielded positive ion CID spectra that exactly matched that of the 13-HpODE-CE standard, whereas the spectra of peaks 3c and 3d matched the spectra of the 9-HpODE-CE standard. The CID of ammoniated HpODE-CEs are rich with structural information, and therefore, these spectra provided support for their identification, as recently reported (31). These oxCEs were readily trimethylsilylated upon treatment with BSTFA (supplementary Fig. III-C). RP-HPLC-MS/MS analyses of hydrolyzed acyl components (compared with authentic HpODE standards) also supported the identification of group 3 peaks as the HpODE-CE isomers indicated in Table 1.

## Group 4 peaks

Group 4 peaks of  $m/z$  698 were consistent with the addition of two oxygen atoms to 18:2-CE (+32 amu) (Fig. 1B). These compounds were significantly more polar than both HpODE-CEs and HODE-CEs and consisted of a mixture of isobaric compounds which all yielded identical product spectra. When group 4 peaks were isolated and treated with BSTFA, the products were exclusively monosilylated (+72 amu), indicating these oxCEs contained only a single hydroxyl (supplementary Fig. III-E). Group 4 peaks were collected, hydrolyzed, and analyzed by RP-HPLC-MS/MS. These experiments revealed a complex mixture of acyl components whose product ion spectra exactly matched previously published product ion spectra of epoxy-hydroxy linoleate components (32). These results indicate that group 4 peaks were hydroxy-epoxy-linoleate-CEs, as shown in Table 1. Double bond geometry and stereochemistry were not determined for this family.

## Group 5 peaks

The ion at  $m/z$  680 was consistent in mass and polarity with an oxo containing 18:2-CE (Fig. 1B). The extracted ion chromatogram revealed peaks at 13, 15, and 17 min. In serial injection experiments, peaks 5a and 5b displayed the similar retention times as synthetic cholesteryl 13-oxo-9Z, 11E-octadecadienoic acid (13-(ZE)-oxoODE) and 9-(EZ)-oxoODE, respectively. All group 5 peaks formed both protonated,  $[M+H]^+$  ( $m/z$  663), and ammoniated,  $[M+NH_4]^+$  ( $m/z$  680), molecular ion species as did the synthetic oxoODE-CE standards. Group 5 peaks were isolated and treated with methoxyamine and readily converted to methoxime species,  $m/z$  679 (+29 amu), confirming the presence of an oxo moiety (supplementary Fig. IV-A). Hydrolyzed acyl components from group 5 peaks were analyzed by RP-HPLC-MS/MS. The results, when compared with authentic standards, were consistent with the oxoODE isomers. The oxoODE-CE species present in human atheromata are indicated in Table 1.

## Group 6 peaks

The ion at  $m/z$  696 was consistent with a series of keto-epoxy- or keto-hydroxy-linoleate-CEs (Fig. 1B). Methoxyamine treatment resulted in conversion to the methoxime species indicated by an increase in mass (+29 amu) and a slight loss of polarity (supplementary Fig. IV-B). These results confirmed the presence of an oxo moiety; however, BSTFA treatment did not produce silylated species, suggesting the second oxygen was not a hydroxyl. An epoxide moiety as the second oxygen would be consistent with these observations. Attempts to hydrolyze these oxCEs and obtain negative ion MS/MS spectra were unsuccessful. Indeed, a recent study found such compounds are unstable during hydrolysis; and therefore, analysis of the saponified acyl chain is not trivial (33). The proposed keto-epoxy-linoleate-CEs observed in human atheromata are listed in Table 1.

## Group 7 peaks

The ion at  $m/z$  706 was consistent with the addition of one oxygen atom to 20:4-CE (Fig. 1B). The extracted ion

chromatogram of  $m/z$  706 revealed a group of peaks with similar retention times as the HODE-CEs. When group 7 peaks were isolated and treated with BSTFA, they readily formed silylated products,  $m/z$  778 (+72 amu) (supplementary Fig. III-B). Group 7 peaks were hydrolyzed and subjected to RP-HPLC-MS/MS. The retention times and CID spectra of the acyl components were consistent with authentic HETE isomers. Double-bond geometries were not determined for this family. The HETE-CE identified in atheromata are listed in Table 1.

## Group 8 peaks

The ion at  $m/z$  722 was consistent with the addition of two oxygen atoms to 20:4-CE (Fig. 1B). The extracted ion chromatogram of  $m/z$  722 showed a group of peaks with similar retention times as the HpODE-CE series. Group 8 peaks were isolated and treated with BSTFA. Like the silylation products of the HpODE-CE family, the silylated products here were monosilylated and eluted just after solvent front (supplementary Fig. III-D). Sufficient quantities of material could not be isolated to allow for RP-HPLC analysis of the saponified acyl components. Group 8 peaks were likely a series of HpETE-CE isomers similar to the HETE-CE family. Using highly sensitive MRM detection provided evidence of a series of corresponding oxoETE-CEs; however, these compounds were at low abundance and could not be characterized confidently.

## Group 9 peaks

Group 9 peaks were significantly more polar than both the HETE-CE series and the HpETE-CE series and showed similar retention times as the hydroxy-epoxy-linoleate-CEs (Fig. 1B). Group 9 peaks were isolated from an atheroma extract and treated with BSFTA. Like the silylation products of the hydroxy-epoxy-linoleate-CEs, the products were exclusively monosilylated (+72 amu) (supplementary Fig. III-F). Polarity was reduced but not eliminated, again similar to the hydroxy-epoxy-linoleate-CEs. Sufficient material was not available for RP-HPLC MS/MS of the acyl components. On the basis of these results and the fact that hydroxy-epoxy-arachidonates are known degradation products of arachidonate peroxidation, group 9 was likely a highly complex mixture of hydroxy-epoxy-arachidonate-CE isomers (34).

## Chain-shortened $\omega$ -oxidized cholesteryl esters

Scanning at lower mass ( $m/z$  420 to 620) for precursors of  $m/z$  369.3 revealed a series of polar compounds eluting during NP-HPLC-MS/MS analyses of atheromata extracts (Fig. 2). The most abundant of these compounds, at  $m/z$  558, was consistent with an ammoniated cholesteryl ester,  $[M+NH_4]^+$ , with an acyl group having nine carbons, no double bonds and a single oxo moiety. Treatment with methoxyamine readily converted this compound to the methoxime species (+29 amu), confirming the oxo moiety (supplementary Fig. IV-C). Less abundant ions were consistent with similar species having acyl components of various chain lengths. Together these compounds were likely

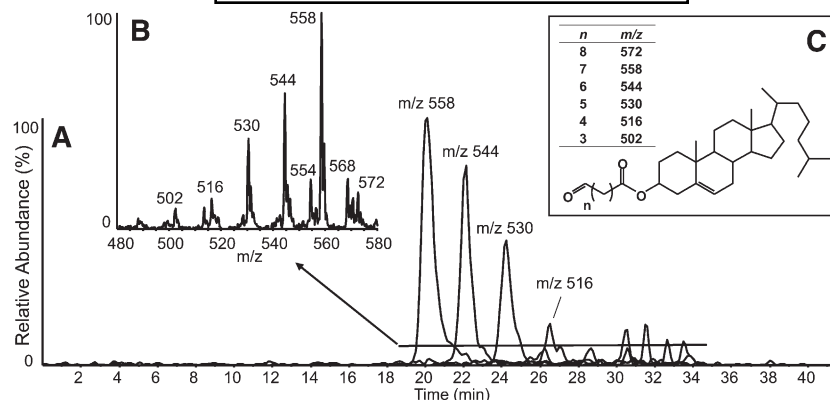


**Fig. 2.** NP-HPLC-MS/MS analysis of cholesteryl esters of chain-shortened,  $\omega$ -oxidized acyl components extracted from human atheroma. (A) Extracted ion chromatograms of the major species. Chromatographic peaks are labeled with the  $m/z$  value extracted. (B) Integrated mass spectrum averaged over the period indicated by the horizontal line. (C) General structure of chain shortened  $\omega$ -oxidized CEs. The table indicates calculated nominal  $m/z$  values of ammoniated species,  $[M+NH_4]^+$ .

a series of  $\omega$ -oxidized, chain-shortened fatty acyl cholesteryl esters, also referred to as core aldehydes. Extracted ion chromatograms of the major ions are shown in Fig. 2A. Longer chain-length species eluted first, and shorter species were eluted later; these results were consistent with previously published reversed-phase separations which showed the opposite elution profile (3, 35). There were also several minor ion species with  $m/z$  values not consistent with this series, e.g.,  $m/z$  554 and 568, although these ions were typically of low abundance (Fig. 2B).

### Esters of oxidized cholesterol

Scanning for precursors of  $m/z$  385.3 (cholesteryl cation+[O]) revealed two major groups of compounds. The late-eluting group (Fig. 3C) had molecular weights consistent with oxidized cholesterol esterified to the typical acyl components esterified to unoxidized CE species (i.e., linoleate, arachidonate, and docosahexaenoic

acid). The relatively high polarity of this family suggested that the oxygen was likely present as a hydroxyl although no further characterization was done. The early-eluting compounds (Fig. 3B) were esterified to a more saturated family of acyl components, with oleic acid (18:1) and eicosatrienoic acid (20:3) being the most abundant acyl species. A less polar oxygen moiety, possibly an epoxy, was likely present on the cholesteryl nucleus in this class of esters. Together, these species had an absolute intensity <10% of unmodified 18:2-CE, although no calibration curves were made for esters of oxidized cholesterol.

### Quantitation of the specific 15-lipoxygenase product in human atheromata

15-LO catalyzes the formation of (*S*)-13-(*ZE*)-HODE-CE from cholesteryl linoleate. The four HODE-CE isomers were well separated by NP-HPLC, and their relative peaks

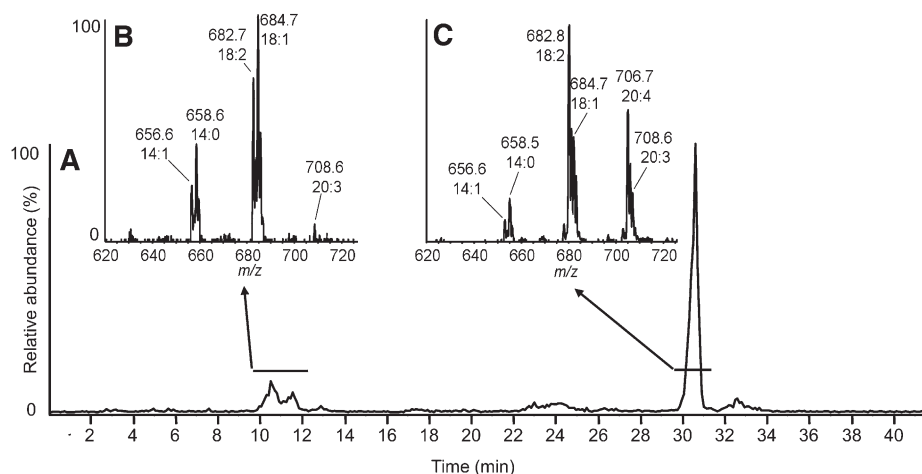


**Fig. 3.** NP-HPLC-MS/MS analysis of fatty acid esters of oxidized cholesterol. (A) Precursors of  $m/z$  385.3 ( $m/z$  620 to 780) total ion chromatogram. (B, C) Integrated mass spectral data averaged over the periods indicated by the horizontal lines. CE species are labeled with  $m/z$  values and their acyl components by total acyl carbons and double bonds.



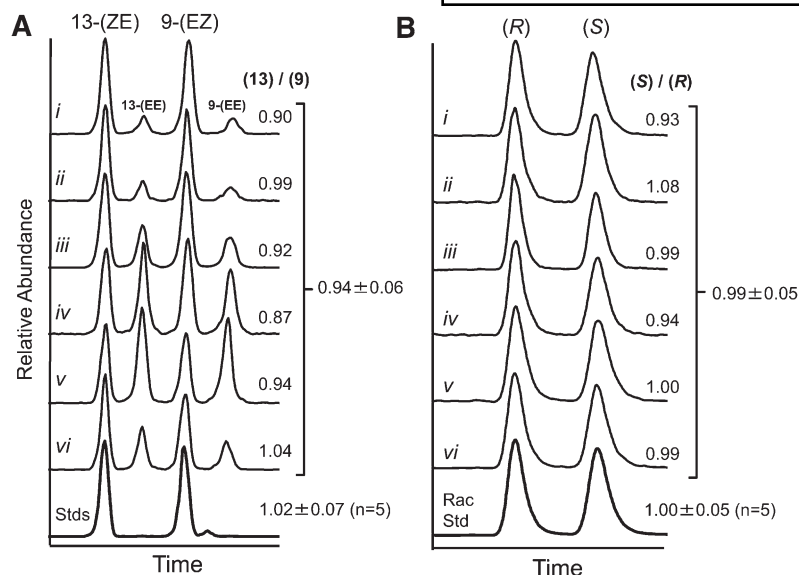


**Fig. 4.** Regio- and stereoselectivity of HODE-CEs extracted from human atheromata. (A) NP-HPLC-MS/MS separation of HODE-CE geometric isomers from six human atheromata. (B) Chiral HPLC-MS/MS separation of (R)- and (S)-13-(ZE)-HODE-CE isolated from the same human atheromata. HODE-CEs were detected by multiple reaction monitoring ( $m/z$  682.6 to 369.3). Roman numerals identify the individual atheromata samples. The indicated abundance ratios were calculated by peak area. Bottom trace show typical chromatograms of authentic standards. Abundance ratio averages  $\pm$  SD are indicated for the six samples and for intraday analyses of authentic standards.

areas were determined by MRM (**Fig. 4A**). The average peak area ratio of 13-(ZE)-HODE-CE / 9-(EZ)-HODE-CE for six atheromata was  $0.94 \pm 0.06$  (mean  $\pm$  SD). Equimolar quantities of authentic standards produced a 13-/9- peak area ratio of  $1.02 \pm 0.07$  (mean  $\pm$  SD,  $n = 5$  intraday measurements). Chiral separations of 13-(ZE)-HODE-CE isolated from each of the six atheromata each produced two peaks that matched the retention times of authentic (+/-)13-(ZE)-HODE-CE (**Fig. 4B**). Analysis of authentic (R)13-(ZE)-HODE-CE revealed the individual enantiomers. The average S/R peak area ratio of the atheromata was  $0.99 \pm 0.05$  (mean  $\pm$  SD), whereas the S/R ratio of the racemic standard was  $1.00 \pm 0.05$  (mean  $\pm$  SD,  $n = 5$  intraday measurements). These results indicated no significant regio- or stereoselectivity in the HODE-CE profile of human atheromata.

#### Extent of cholesteryl ester oxidation

To more accurately determine the relative quantities of the three major CE species (18:2-CE, 20:4-CE, and 22:6-CE) and their oxidation products, human atheromata extracts were spiked with the internal standard 17:1-CE and analyzed by NP-HPLC-MS/MS using MRM. After generating calibration curves, the relative abundances of the major CEs and their oxidation products were determined for each of the six human atheromata and pooled human plasma. As expected, cholesteryl linoleate and its oxidation products were by far the most abundant species, followed by cholesteryl arachidonate and cholesteryl docosahexaenoate and their oxidation products (**Fig. 5**). Across the six samples, the 18:2-CE pool was an average of  $23 \pm 13\%$  oxidized, the 20:4-CE pool was  $16 \pm 6\%$  oxidized, the 22:6-CE pool was  $12 \pm 4\%$  oxidized, and the total CE pool was  $21 \pm 11\%$  oxidized (mean  $\pm$  SD). Cholesteryl linoleate was the most oxidized CE species on a per-sample basis ( $P = <0.001$  compared with 20:4-CE;  $P < 0.005$  compared with 22:6-CE). The pooled plasma sample had a typical CE profile, in agreement with previous studies, and

showed very little oxidation; however, some of the more abundant oxCE species, such as HODE-CEs and HpODE-CEs, were detected (36).

#### IMS of human atherosclerotic plaques

To determine the localization of neutral lipid species in plaques prior to extraction, 20  $\mu$ m slices of human atheromata were prepared and imaged by MALDI IMS. These analyses revealed abundant ions with  $m/z$  values consistent with sodium adducts of the major CEs and oxCEs within the plaques (**Fig. 6K, L**). MALDI-TOF product ion spectra obtained directly from tissue slices or from authentic standards confirmed the identity of major CEs and oxCEs (**Fig. 7**). Interestingly, CID of the CE sodium adducts yielded very different spectra than their ammoniated counterparts. While ammoniated CEs yielded an abundant  $m/z$  369.3, sodiated CEs yielded little  $m/z$  369, instead showing strong ions corresponding to sodiated acyl components, e.g.,  $m/z$  319 in the HODE-CE spectra (**Fig. 7C, G**). The identities of major TAGs and phospholipids were also confirmed by MALDI-TOF-MS/MS (data not shown). All neutral lipid species were exclusively observed as sodium adducts, whereas phospholipids were observed as sodiated and protonated ion species.

CEs and oxCEs were colocalized exclusively within plaques, with 18:2-CE being the most abundant ion in these regions (**Fig. 6D, I, K, L**). Phospholipids, mainly palmitoyl-sphingomyelin and various glycerylphosphocholine species, were also observed within the lesion, but they were more intense in other areas, such as media, adventitia, and extravascular adipose (**Fig. 6A, F, D, I**). Triacylglycerides, as expected, were the most abundant ions in extravascular adipose (data not shown), but they were also present at lower levels in the lesion area. When spectra obtained specifically from the plaque regions were integrated, TAGs and certain phospholipids were present; however, CEs were consistently the most intense ions observed (**Fig. 6K, L**).



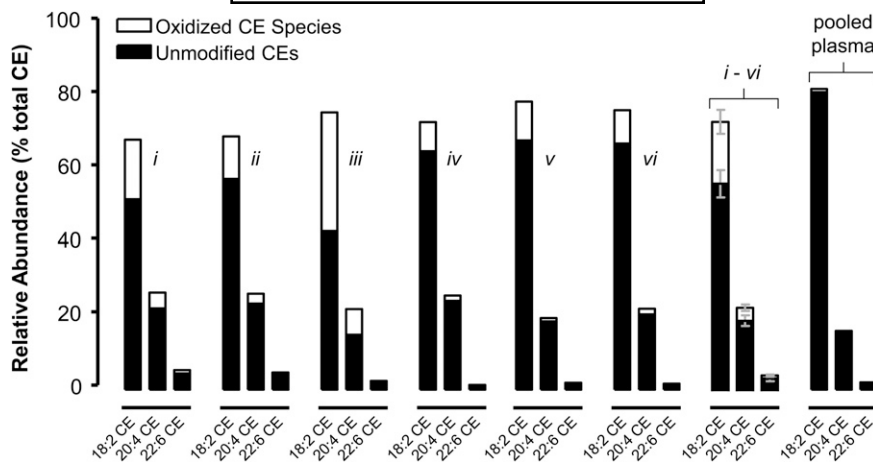


**Fig. 5.** Extent of cholesteryl ester oxidation in human atheromata. Relative quantitation was assessed by NP-HPLC-MS/MS as described in Experimental Procedures. Solid bars indicate the relative abundance of the three major CE species; the summed oxidation products of each CE species are indicated by open bars. Roman numerals indicate individual atheromata, the same samples shown in Fig. 4. The “*i-vi*” graph shows the average  $\pm$  SD of the six atheromata samples. Pooled plasma was derived from 22 healthy donors. Oxidation levels in plasma were too low to appear clearly in this format; however, oxCE were detected at low levels in pooled plasma.

## DISCUSSION

### Oxidized cholesterol esters in human peripheral vascular lesions

Historically, oxCE analyses relied on HPLC-UV monitoring absorbance at 235 nm. This method is sensitive for the detection of lipid species that contain a conjugated diene (i.e., HODE-CEs); however, is not well suited for other species (e.g., EpOME-CEs or unoxidized CEs (5, 22)). To detect a wider variety of species, these analyses leveraged the predictable CID behavior of ammoniated CEs. Regardless of the acyl chain, these species all produce a strong ion at  $m/z$  369 (cholesteryl cation) following CID. Because of this common product ion, precursor ion scanning (precursors of  $m/z$  369) is selective for cholesteryl esters and not significantly biased for any particular acyl chain. This detection method revealed a complex array of abundant oxCE species in extracts of vascular plaques from human femoral and popliteal arteries. It was immediately apparent that the number of individual species and their relative abundances were beyond that previously reported. Although the amount CE oxidation varied between atheromata (Fig. 5), the array of species observed (Table 1) was remarkably consistent. The oxCE pool was composed of many families of isobaric compounds; indeed, every ion observed produced multiple peaks in the chromatogram. The presence of tightly grouped peaks suggested that some families were structurally related regioisomers that likely contained the same oxygen moiety [e.g., HODE-CEs ( $m/z$  682)]. There were also independent families, each containing several compounds, all of which were isobaric [e.g., HODE-CEs and EpOME-CEs (both  $m/z$  682)].

With the notable exception of the HpODE-CE species, positive ion CID spectra of ammoniated oxCEs were structurally uninformative (31). CID of the sodium adducts

produced different, but equally uninformative, product ion spectra (Fig. 7). Therefore, negative ion MS/MS of the hydrolyzed acyl anions were often critical for structural determination. These experiments were particularly useful because negative ion CID spectra of oxidized fatty acids yield structurally relevant product ions, and these spectra have been well studied (32, 37, 38). For example, the regioisomers of the HETE-CE series could only be confidently assigned after negative ion MS/MS of the acyl components were obtained and compared with CID authentic standards and previously published spectra. Negative ion MS/MS was also critical for the characterization of the epoxy-hydroxy-linoleate-CE.

Derivatization approaches, such as trimethylsilylation, were useful for determining the number and type of functional groups present. For example, the hydroxy-epoxy-linoleate-CEs were originally hypothesized to be dihydroxy-linoleate-CEs; however, upon treatment with the silylating reagent BSTFA, strictly monosilylated products were produced, indicating that only a single free hydroxyl was present (supplementary Fig. IV-E). Derivatization with methoxyamine was critical for determining which species contained an oxo moiety by observing their conversion to the methoxime (supplementary Fig. IV). For example, the keto-epoxy-linoleate-CEs were a complex mixture of compounds, each present at very low abundance. Therefore an approach which yielded information regarding the entire family (i.e., that they all contained a ketone) was an important step toward characterizing these species.

Cholesteryl esters of  $\omega$ -oxidized, terminal-aldehyde fatty acyl components, or core aldehydes, also produce the diagnostic  $m/z$  369 ion upon CID. These species were detected using essentially the same methods that were used to detect longer chain fatty acyl groups. The  $m/z$  values observed in these analyses were consistent with cholesteryl

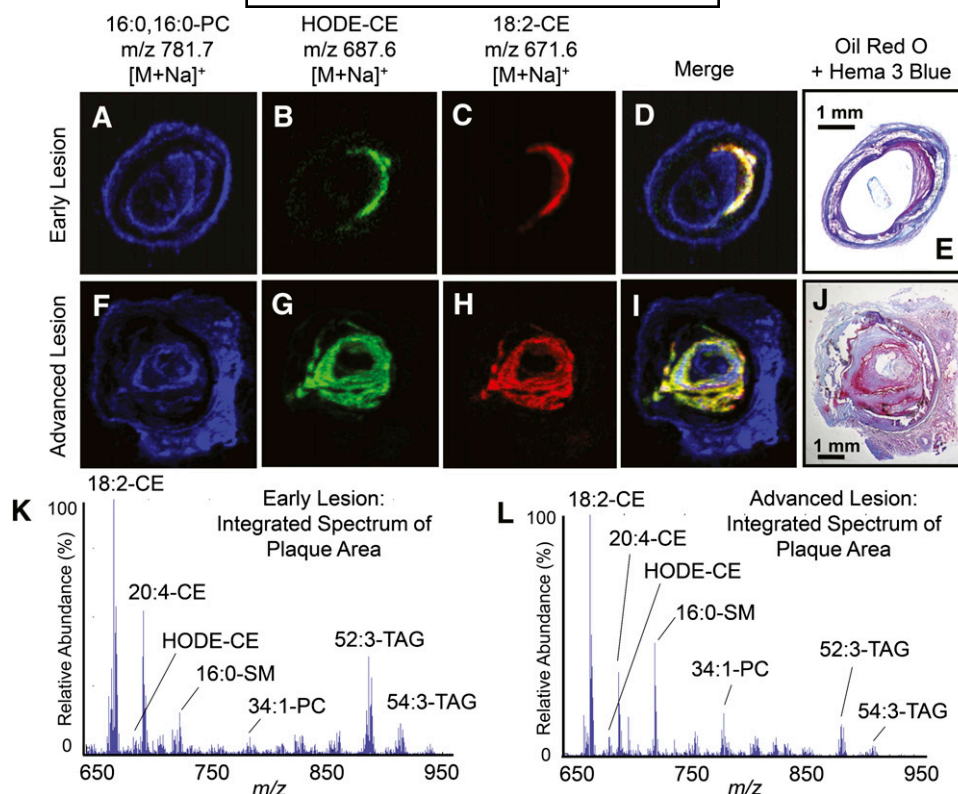


**Fig. 6.** MALDI IMS analysis of CE and oxCE in human arteries with atherosclerotic lesions. Extracted positive ion MALDI images of sodiated (A, F) dipalmitoylphosphatidylcholine  $m/z$  781.7, (B–G) HODE-CE  $m/z$  687, and (C, H) 18:2-CE  $m/z$  671. (D, I) Merged positive ion MALDI image of all three ions indicated above. IMS ion intensities are indicated by color intensities, which were independently scaled for each panel. (E, J) Adjacent slices stained with Oil Red O and Hema 3<sup>®</sup> blue as described in Experimental Procedures. (K, L) Integrated MALDI-TOF spectra summed over the specific lesion areas within the arteries. The major ions are labeled by total acyl carbons, total double bonds, and lipid class; all labeled species are sodium adducts,  $[M+Na]^+$ .

esters of  $\omega$ -oxidized acyl components of various chain lengths (Fig. 2B, C). Some of these species have been identified previously in human atheromata and have been shown to form complexes with, and covalently bind to, proteins (3, 39). Cholesteryl esters, oxidized in the cholesterol nucleus, were also observed but in lower abundance (Fig. 3).

### Novel cholesteryl ester oxidation products

Various oxidized lipids, including many with the structural features found in these oxidized cholesteryl esters isolated from human atherosclerotic plaques, are known to have significant biological activities. Biological activity has been found with intact cholesteryl esters as well as oxidized fatty acids that would be derived following ester hydrolysis. Experimentally oxidized 20:4-CE by 15-lipoxygenase (immobilized soybean 15-LO) was found to activate macrophages and cause release of proinflammatory cytokines (40). Cellular responses to oxCE may be mediated through interactions with toll-like receptor-4 (41). This oxidized 20:4-CE was shown to contain many of the products described in this study. Although present at low abundance, singly and doubly oxidized products of 22:6-CE were also detected in the atherosclerotic plaque

samples using sensitive MRM detection (data not shown). Thus, a large number of very different oxidized fatty acyl-cholesteryl esters are present in plaque that could be substrates for esterases to release diverse oxylipins. Such free fatty acids are known to express a host of activities, including HODEs from linoleate oxidation causing pain (42), anti-inflammatory epoxy-hydroxy products (i.e., hepoxilins) (43, 44), EpOMes (i.e., leukotoxins) from linoleate (45, 46), products of 22:6 oxidation known as anti-inflammatory maresins (47), and perhaps most relevant, various HETEs and 13-HODE as ligands for PPAR- $\gamma$  driving expression of CD36, a receptor for oxLDL (48–51).

### Extent of cholesteryl ester oxidation in human atheromata

Previous studies reported that up to 30% of the cholesteryl linoleate in atheromata was present in oxidized form; however, these studies were unable to detect many of the oxCE species we observed by NP-HPLC-MS/MS (5). Initial experiments suggested that a larger proportion of cholesteryl linoleate was oxidized and that cholesteryl arachidonate and cholesteryl docosahexaenoate were also oxidized. Because the precursor ion scanning experiment required a relatively slow sampling rate, we used MRM for oxCE

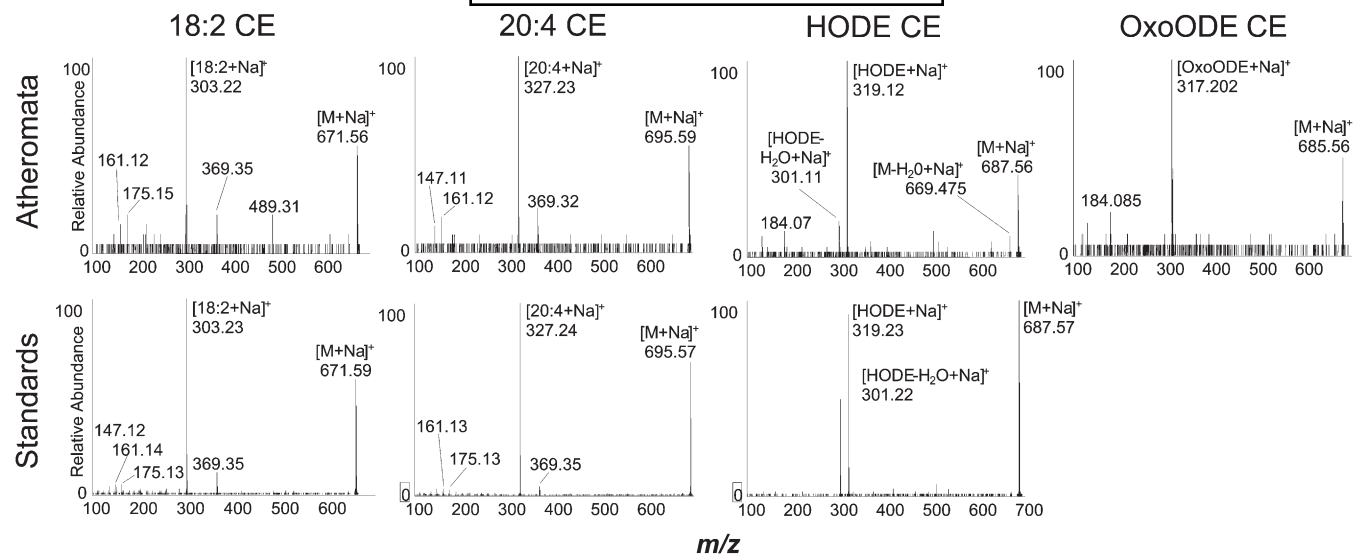


**Fig. 7.** MALDI-TOF product ion spectra of CEs and oxCEs acquired from human atheromata and authentic standards. The species selected for CID is indicated above the spectra; the source of the compound is indicated to the left. Upper panels: CID spectra acquired from human atheromata tissue sections prepared as described in "Experimental Procedures." Lower panels: CID spectra acquired from authentic standards dried onto the MALDI plate, layered with NaCl and sublimed DHB matrix as described in Experimental Procedures. An authentic standard for oxoODE-CE was not available.

quantitation. After constructing calibration curves, it was determined that up to 45% of the 18:2-CE pool in human atheromata was present in oxidized form; however, most samples showed closer to 25% 18:2-CE oxidation ( $23 \pm 13\%$ , mean  $\pm$  SD). Cholesteryl linoleate was the most oxidized of the three major CE species; this observation was consistent with cholesteryl linoleate being the preferred substrate of 15-LO, although further analysis did not detect a preponderance of the specific 15-LO oxidation product (Fig. 4).

When the oxidized and unoxidized CEs were summed, the relative amounts of the three most abundant CEs, 18:2-CE, 20:4-CE and 22:6-CE, were similar to the relative amounts detected in human plasma; however, the level of CE oxidation in plasma was far less than in atheromata. These results suggested either that oxCE was selectively accumulated in the atheromata or that CE from the blood was oxidized within the lesion. It has been shown that HDL is the major carrier of oxCE in the blood, not LDL, which is the particle associated with lesion formation (52). Considering this, it is likely that CE from the circulation is accumulated and oxidatively modified within the lesion to some degree, perhaps extensively.

#### Relative quantitation of 15-LO-specific CE oxidation product

Several studies have investigated the role of 15-LO in CE oxidation by interrogating atheromata for the specific enzymatic oxidation product (*S*)13-(ZE)-HpODE-CE or its reduction product (*S*)13-(ZE)-HODE-CE. These efforts have yielded conflicting results. A large study of 80 human atheromata reported a slight preponderance of (*S*)13-HODE-CE after hydrolysis and methylation (*S/R* ratio of 1.12) (21). A study interrogating the stereospecificity of

13-HODE in linoleic acid-fed rabbits and in human atheromata reported a convincing preponderance of (*S*)13-HODE in linoleate-fed rabbits at early time points (which was reduced over time), but it found no stereospecificity in human samples (20). Several investigations of the regioisomers of HODE-CE in human atheromata and in human plasma found no excess oxygenation at carbon 13 and did not implicate 15-LO (5, 22, 53). No chiral separations of intact oxCE have been reported previously; therefore, direct analysis of oxCEs from human samples has not been done. Here, normal-phase and chiral-phase HPLC-MS/MS analysis of six human atheromata determined the regio- and stereospecificity of the HODE-CEs as intact species.

When the four regioisomers of HODE-CE were separated by NP-HPLC-MS/MS, the peak areas of 13-(ZE)-HODE-CE and 9-(ZE)-HODE-CE was essentially equal (Fig. 4A). No sample had a 13-/9- ratio above the 95% confidence interval (CI) of the authentic standards (95% CI = 0.93 to 1.11). The 13-(ZE)-HODE-CE regioisomer was then isolated by preparative NP-HPLC-MS/MS and separated by chiral chromatography. The (*S*)- and (*R*)13-(ZE)-HODE-CE peak areas were once again essentially equal with only a single sample (Fig. 4B-ii) having an *S/R* ratio above the 95% CI of the racemic standard (95% CI = 0.95 to 1.05). Over time, nonspecific products observed during *in vitro* 15-LO-catalyzed CE oxidation are known to increase relative to (*S*)13-(ZE)-HODE-CE, and this process erodes the specificity of the product profile (17). In the context of these observations, our results may not necessarily rule out 15-LO as an initiating event leading to oxCE in human atheromata, especially considering that human vascular disease develops over many decades. It is likely that nonenzymatic mechanisms (likely radical driven) predominate over time.




## Localization of oxidized cholesteryl esters in human atheromata

Homogenization and extraction of whole atheromata, the most common technique for lipid analysis, destroys information regarding the in situ distribution of plaque components. An advantage of IMS is its ability to provide spatial information about molecules that cannot be visualized by other techniques. This is particularly true for lipids, where IMS has revealed the distributions of various lipids in different tissues (54, 55). Surprisingly, IMS studies of atheromata are exceedingly scarce, and none has reported the detection of oxCEs (56, 57). Thus, it remained unclear whether oxCEs were concentrated in specific areas of atheromata, such as the necrotic core, or the shoulder regions where there is more cellularity.

To determine the localization of oxCE species in human atheromata, we analyzed atherosclerotic human arteries by MALDI-IMS. These studies revealed the distribution of CEs, oxCEs, and many other lipid species. The lipids observed and their relative abundance was highly dependent on the anatomical region examined. In areas composed mainly of calcified material, few ions were detected and no lipids were observed. Triacylglycerides were mainly observed in the extravascular adipose but also within the plaque, although at lower abundances. Phospholipids (e.g., dipalmitoyl-phosphocholine) were observed throughout the arteries and were therefore useful as anatomical landmarks when interpreting IMS. Cholesteryl esters and oxCEs were completely localized within the plaque (Fig. 6B, C, G, H, K, L). Sodium adducts of these species,  $[M+Na]^+$ , were by far the most abundant ions within the lesions, but they were not observed at all in other anatomical regions. Extracted ion images of 18:2-CE and HODE-CE indicated these species had essentially identical spatial distributions exclusively within the plaque (Fig. 6D, I). These results suggested that CE oxidation occurred throughout the lesion because oxCEs were not concentrated in any particular region of the plaques.

It was also notable that TAGs were observed in the plaque as rather abundant ions (Fig. 6K, L). This was a curious observation as no oxidized TAGs were detected in atheromata extracts by MALDI-IMS or by HPLC-MS/MS (supplementary Fig. V). This was the case even for atheromata that showed over 40% oxidation of the CE pool. In control experiments, oxTAG species, formed by treating plaque extracts with ozone, were readily observed by HPLC-MS/MS, confirming that oxTAGs, when present, are detectable by these methods (supplementary Fig. VI). These results indicate that TAGs and CEs, while both present in the lesion, were oxidized differently and suggest that CE oxidation is somewhat specific. If oxidative processes in the atheromata were purely nonselective, one would reasonably expect to find evidence of polyunsaturated TAG oxidation in plaque samples where oxCEs were clearly evident. Mechanisms of selective oxCE accumulation include enzymatic CE oxidation (e.g., 15-LO), selective uptake of oxCE, incomplete remodeling of oxCE (compared with oxTAG), and physical separation of CE and TAG at a scale unresolved by IMS.

In summary, cholesteryl ester oxidation in human atheromata resulted in an array of oxCEs more abundant and diverse than previously appreciated. This family of lipids included oxidation products of the major CE species present in human plasma, and several novel oxCE species were identified. Quantitative measurements determined that, on average,  $21 \pm 11\%$  (mean  $\pm$  SD) of the CE pool was present in oxidized form, with one sample showing over 40% oxidation. These analyses also revealed that 18:2-CE was oxidized to a greater extent than other CE species. IMS revealed that oxCEs were localized entirely within the lesion area and had a nearly identical spatial distribution as unmodified CEs. Triacylglycerides were also present within the lesion; however, polyunsaturated TAG species showed no evidence of oxidative modification. Selective oxidation of 18:2-CE and an absence of TAG oxidation were observations consistent with 15-LO activity; however, further analyses of HODE-CEs indicated no preponderance of the specific 15-LO oxidation product. This result suggested that either 15-LO is not a major source of oxCE in human atheromata or the generation nonspecific products overwhelmed the oxCE profile. This situation could occur through "seeding," in which peroxide products of 15-LO initiate further oxidation, or by intermolecular isomerization and racemization of direct 15-LO oxidation products; both mechanisms would invoke nonspecific radical chemistry. 

The authors thank Dr. David W. Russel for providing the pooled human plasma sample. The authors also thank Drs. Max Wohlauser and Jeffery Harr for assisting in the collection of human atheromata samples.

## REFERENCES

1. Glavind, J., and S. Hartmann. 1951. The occurrence of peroxidized lipids in atheromatous human aortas. *Experientia*. **7**: 464.
2. Glavind, J., S. Hartmann, J. Clemmesen, K. E. Jessen, and H. Dam. 1952. Studies on the role of lipoperoxides in human pathology. II. The presence of peroxidized lipids in the atherosclerotic aorta. *Acta Pathol. Microbiol. Scand.* **30**: 1–6.
3. Hoppe, G., A. Ravandi, D. Herrera, A. Kuksis, and H. F. Hoff. 1997. Oxidation products of cholesteryl linoleate are resistant to hydrolysis in macrophages, form complexes with proteins, and are present in human atherosclerotic lesions. *J. Lipid Res.* **38**: 1347–1360.
4. Suarna, C., R. T. Dean, J. May, and R. Stocker. 1995. Human atherosclerotic plaque contains both oxidized lipids and relatively large amounts of alpha-tocopherol and ascorbate. *Arterioscler. Thromb. Vasc. Biol.* **15**: 1616–1624.
5. Suarna, C., R. T. Dean, P. T. Southwell-Keeley, D. E. Moore, and R. Stocker. 1997. Separation and characterization of cholesteryl oxo- and hydroxy-linoleate isolated from human atherosclerotic plaque. *Free Radic. Res.* **27**: 397–408.
6. Karten, B., H. Boechzelt, P. M. Abuja, M. Mittelbach, K. Oettl, and W. Sattler. 1998. Femtomole analysis of 9-oxononanoyl cholesterol by high performance liquid chromatography. *J. Lipid Res.* **39**: 1508–1519.
7. Brown, M. S., and J. L. Goldstein. 1983. Lipoprotein metabolism in the macrophage: implications for cholesterol deposition in atherosclerosis. *Annu. Rev. Biochem.* **52**: 223–261.
8. Steinberg, D. 2009. The LDL modification hypothesis of atherogenesis: an update. *J. Lipid Res.* **50**(Suppl.): S376–S381.
9. Skipski, V. P., M. Barclay, R. K. Barclay, V. A. Fetzter, J. J. Good, and F. M. Archibald. 1967. Lipid composition of human serum lipoproteins. *Biochem. J.* **104**: 340–352.

10. Upston, J. M., X. Niu, A. J. Brown, R. Mashima, H. Wang, R. Senthilmohan, A. J. Kettle, R. T. Dean, and R. Stocker. 2002. Disease stage-dependent accumulation of lipid and protein oxidation products in human atherosclerosis. *Am. J. Pathol.* **160**: 701–710.
11. Yamamoto, Y., M. H. Brodsky, J. C. Baker, and B. N. Ames. 1987. Detection and characterization of lipid hydroperoxides at picomole levels by high-performance liquid chromatography. *Anal. Biochem.* **160**: 7–13.
12. Folcik, V. A., and M. K. Cathcart. 1994. Predominance of esterified hydroperoxy-linoleic acid in human monocyte-oxidized LDL. *J. Lipid Res.* **35**: 1570–1582.
13. Henriksen, T., E. M. Mahoney, and D. Steinberg. 1981. Enhanced macrophage degradation of low density lipoprotein previously incubated with cultured endothelial cells: recognition by receptors for acetylated low density lipoproteins. *Proc. Natl. Acad. Sci. USA.* **78**: 6499–6503.
14. Belkner, J., P. Chaitidis, H. Stender, C. Gerth, R. J. Kuban, T. Yoshimoto, and H. Kuhn. 2005. Expression of 12/15-lipoxygenase attenuates intracellular lipid deposition during in vitro foam cell formation. *Arterioscler. Thromb. Vasc. Biol.* **25**: 797–802.
15. Weibel, G. L., M. R. Joshi, E. T. Alexander, P. Zhu, I. A. Blair, and G. H. Rothblat. 2009. Overexpression of human 15(S)-lipoxygenase-1 in RAW macrophages leads to increased cholesterol mobilization and reverse cholesterol transport. *Arterioscler. Thromb. Vasc. Biol.* **29**: 837–842.
16. Fang, L., R. Harkewicz, K. Hartvigsen, P. Wiesner, S-H. Choi, F. Almazan, J. Pattison, E. Deer, T. Sayaphupha, E. A. Dennis, et al. 2010. Oxidized cholesteryl esters and phospholipids in zebrafish larvae fed a high cholesterol diet: macrophage binding and activation. *J. Biol. Chem.* **285**: 32343–32351.
17. Belkner, J., H. Stender, and H. Kuhn. 1998. The rabbit 15-lipoxygenase preferentially oxygenates LDL cholesterol esters, and this reaction does not require vitamin E. *J. Biol. Chem.* **273**: 23225–23232.
18. Belkner, J., R. Wiesner, H. Kuhn, and V. Z. Lankin. 1991. The oxygenation of cholesterol esters by the reticulocyte lipoxygenase. *FEBS Lett.* **279**: 110–114.
19. Ylä-Herttuala, S., M. E. Rosenfeld, S. Parthasarathy, C. K. Glass, E. Sigal, J. L. Witztum, and D. Steinberg. 1990. Colocalization of 15-lipoxygenase mRNA and protein with epitopes of oxidized low density lipoprotein in macrophage-rich areas of atherosclerotic lesions. *Proc. Natl. Acad. Sci. USA.* **87**: 6959–6963.
20. Kuhn, H., J. Belkner, S. Zaiss, T. Fahrenklemp, and S. Wohlfeil. 1994. Involvement of 15-lipoxygenase in early stages of atherogenesis. *J. Exp. Med.* **179**: 1903–1911.
21. Folcik, V. A., R. A. Nivar-Aristy, L. P. Krajewski, and M. K. Cathcart. 1995. Lipoxygenase contributes to the oxidation of lipids in human atherosclerotic plaques. *J. Clin. Invest.* **96**: 504–510.
22. Mashima, R., K. Onodera, and Y. Yamamoto. 2000. Regioisomeric distribution of cholesteryl linoleate hydroperoxides and hydroxides in plasma from healthy humans provides evidence for free radical-mediated lipid peroxidation in vivo. *J. Lipid Res.* **41**: 109–115.
23. Luthria, D. L., and H. Sprecher. 1995. Metabolism of deuterium-labeled linoleic, 6,9,12-octadecatrienoic, 8,11,14-eicosatrienoic, and arachidonic acids in the rat. *J. Lipid Res.* **36**: 1897–1904.
24. Hutchins, P. M., R. M. Barkley, and R. C. Murphy. 2008. Separation of cellular nonpolar neutral lipids by normal-phase chromatography and analysis by electrospray ionization mass spectrometry. *J. Lipid Res.* **49**: 804–813.
25. Gijón, M. A., S. Zarini, and R. C. Murphy. 2007. Biosynthesis of eicosanoids and transcellular metabolism of leukotrienes in murine bone marrow cells. *J. Lipid Res.* **48**: 716–725.
26. Furbee, J. W., Jr., J. K. Sawyer, and J. S. Parks. 2002. Lecithin:cholesterol acyltransferase deficiency increases atherosclerosis in the low density lipoprotein receptor and apolipoprotein E knockout mice. *J. Biol. Chem.* **277**: 3511–3519.
27. Harrison, K. A., S. S. Davies, G. K. Marathe, T. McIntyre, S. Prescott, K. M. Reddy, J. R. Falck, and R. C. Murphy. 2000. Analysis of oxidized glycerophosphocholine lipids using electrospray ionization mass spectrometry and microderivatization techniques. *J. Mass Spectrom.* **35**: 224–236.
28. Berry, K. A. Z., B. Li, S. D. Reynolds, R. M. Barkley, M. A. Gijón, J. A. Hankin, P. M. Henson, and R. C. Murphy. 2011. MALDI imaging MS of phospholipids in the mouse lung. *J. Lipid Res.* **52**: 1551–1560.
29. Hankin, J. A., R. M. Barkley, and R. C. Murphy. 2007. Sublimation as a method of matrix application for mass spectrometric imaging. *J. Am. Soc. Mass Spectrom.* **18**: 1646–1652.
30. Kenar, J. A., C. M. Havrilla, N. A. Porter, J. R. Guyton, S. A. Brown, K. F. Klemp, and E. Selinger. 1996. Identification and quantification of regioisomeric cholesteryl linoleate hydroperoxides in oxidized human low density lipoprotein and high density lipoprotein. *Chem. Res. Toxicol.* **9**: 737–744.
31. Hutchins, P. M., and R. C. Murphy. 2011. Peroxide bond driven dissociation of hydroperoxy-cholesterol esters following collision induced dissociation. *J. Am. Soc. Mass Spectrom.* **22**: 867–874.
32. Oliu, E. H., U. Garscha, T. Nilsson, and M. Cristea. 2006. Payne rearrangement during analysis of epoxyalcohols of linoleic and alpha-linolenic acids by normal phase liquid chromatography with tandem mass spectrometry. *Anal. Biochem.* **354**: 111–126.
33. Zheng, Y., H. Yin, W. E. Boeglin, P. M. Elias, D. Crumrine, D. R. Beier, and A. R. Brash. 2011. Lipoxygenases mediate the effect of essential fatty acid in skin barrier formation: a proposed role in releasing omega-hydroxyceramide for construction of the corneocyte lipid envelope. *J. Biol. Chem.* **286**: 24046–24056.
34. Schneider, C., W. E. Boeglin, H. Yin, N. A. Porter, and A. R. Brash. 2008. Intermolecular peroxy radical reactions during autoxidation of hydroxy and hydroperoxy arachidonic acids generate a novel series of epoxidized products. *Chem. Res. Toxicol.* **21**: 895–903.
35. Kamido, H., A. Kuksis, L. Marai, and J. J. Myher. 1992. Identification of cholesterol-bound aldehydes in copper-oxidized low density lipoprotein. *FEBS Lett.* **304**: 269–272.
36. Quehenberger, O., A. M. Armando, A. H. Brown, S. B. Milne, D. S. Myers, A. H. Merrill, S. Bandyopadhyay, K. N. Jones, S. Kelly, R. L. Shaner, et al. 2010. Lipidomics reveals a remarkable diversity of lipids in human plasma. *J. Lipid Res.* **51**: 3299–3305.
37. Murphy, R. C., R. M. Barkley, K. Zemski Berry, J. Hankin, K. Harrison, C. Johnson, J. Krank, A. McAnoy, C. Uhlson, and S. Zarini. 2005. Electrospray ionization and tandem mass spectrometry of eicosanoids. *Anal. Biochem.* **346**: 1–42.
38. Hall, L. M., and R. C. Murphy. 1998. Electrospray mass spectrometric analysis of 5-hydroperoxy and 5-hydroxyeicosatetraenoic acids generated by lipid peroxidation of red blood cell ghost phospholipids. *J. Am. Soc. Mass Spectrom.* **9**: 527–532.
39. Kawai, Y., A. Saito, N. Shibata, M. Kobayashi, S. Yamada, T. Osawa, and K. Uchida. 2003. Covalent binding of oxidized cholesteryl esters to protein: implications for oxidative modification of low density lipoprotein and atherosclerosis. *J. Biol. Chem.* **278**: 21040–21049.
40. Harkewicz, R., K. Hartvigsen, F. Almazan, E. A. Dennis, J. L. Witztum, and Y. I. Miller. 2008. Cholesteryl ester hydroperoxides are biologically active components of minimally oxidized low density lipoprotein. *J. Biol. Chem.* **283**: 10241–10251.
41. Choi, S-H., R. Harkewicz, J. H. Lee, A. Boullier, F. Almazan, A. C. Li, J. L. Witztum, Y. S. Bae, and Y. I. Miller. 2009. Lipoprotein accumulation in macrophages via toll-like receptor-4-dependent fluid phase uptake. *Circ. Res.* **104**: 1355–1363.
42. Patwardhan, A. M., A. N. Akopian, N. B. Ruparel, A. Diogenes, S. T. Weintraub, C. Uhlson, R. C. Murphy, and K. M. Hargreaves. 2010. Heat generates oxidized linoleic acid metabolites that activate TRPV1 and produce pain in rodents. *J. Clin. Invest.* **120**: 1617–1626.
43. Pace-Asciak, C. R. 2009. The hepoxilins and some analogues: a review of their biology. *Br. J. Pharmacol.* **158**: 972–981.
44. Nigam, S. 2007. Hepoxilins: novel enzymatic pathways and clinical significance. *FEBS J.* **274**: 3493.
45. Harris, T. R., P. A. Aronov, P. D. Jones, H. Tanaka, M. Arand, and B. D. Hammock. 2008. Identification of two epoxide hydrolases in *Caenorhabditis elegans* that metabolize mammalian lipid signaling molecules. *Arch. Biochem. Biophys.* **472**: 139–149.
46. Ishizaki, T., T. Ozawa, and N. F. Voelkel. 1999. Leukotoxins and the lung. *Pulm. Pharmacol. Ther.* **12**: 145–155.
47. Serhan, C. N., R. Yang, K. Martinod, K. Kasuga, P. S. Pillai, T. F. Porter, S. F. Oh, and M. Spite. 2009. Maresins: novel macrophage mediators with potent antiinflammatory and proresolving actions. *J. Exp. Med.* **206**: 15–23.
48. Tontonoz, P., L. Nagy, J. G. Alvarez, V. A. Thomazy, and R. M. Evans. 1998. PPARgamma promotes monocyte/macrophage differentiation and uptake of oxidized LDL. *Cell.* **93**: 241–252.
49. Nagy, L., P. Tontonoz, J. G. Alvarez, H. Chen, and R. M. Evans. 1998. Oxidized LDL regulates macrophage gene expression through ligand activation of PPARgamma. *Cell.* **93**: 229–240.
50. Nozaki, S., H. Kashiwagi, S. Yamashita, T. Nakagawa, B. Kostner, Y. Tomiyama, A. Nakata, M. Ishigami, J. Miyagawa, and K. Kameda-Takemura. 1995. Reduced uptake of oxidized low density lipoproteins in monocyte-derived macrophages from CD36-deficient subjects. *J. Clin. Invest.* **96**: 1859–1865.

51. Huang, J. T., J. S. Welch, M. Ricote, C. J. Binder, T. M. Willson, C. Kelly, J. L. Witztum, C. D. Funk, D. Conrad, and C. K. Glass. 1999. Interleukin-4-dependent production of PPAR-gamma ligands in macrophages by 12/15-lipoxygenase. *Nature*. **400**: 378–382.
52. Bowry, V. W., K. K. Stanley, and R. Stocker. 1992. High density lipoprotein is the major carrier of lipid hydroperoxides in human blood plasma from fasting donors. *Proc. Natl. Acad. Sci. USA*. **89**: 10316–10320.
53. Kühn, H., J. Belkner, R. Wiesner, T. Schewe, V. Z. Lankin, and A. K. Tikhaze. 1992. Structure elucidation of oxygenated lipids in human atherosclerotic lesions. *Eicosanoids*. **5**: 17–22.
54. Chughtai, K., and R. M. A. Heeren. 2010. Mass spectrometric imaging for biomedical tissue analysis. *Chem. Rev.* **110**: 3237–3277.
55. Fernández, J. A., B. Ochoa, O. Fresnedo, M. T. Giralt, and R. Rodríguez-Puertas. 2011. Matrix-assisted laser desorption ionization imaging mass spectrometry in lipidomics. *Anal. Bioanal. Chem.* **401**: 29–51.
56. Manicke, N. E., M. Nefliu, C. Wu, J. W. Woods, V. Reiser, R. C. Hendrickson, and R. G. Cooks. 2009. Imaging of lipids in atheroma by desorption electrospray ionization mass spectrometry. *Anal. Chem.* **81**: 8702–8707.
57. Zaima, N., T. Sasaki, H. Tanaka, X. W. Cheng, K. Onoue, T. Hayasaka, N. Goto-Inoue, H. Enomoto, N. Unno, M. Kuzuya, et al. 2011. Imaging mass spectrometry-based histopathologic examination of atherosclerotic lesions. *Atherosclerosis*. **217**: 427–432.